Anisotropic Heat Transfer of Single-Walled Carbon Nanotubes[*]

Shigeo MARUYAMA[**], Yasuhiro IGARASHI[**], Yuki TANIGUCHI[**] and Junichiro SHIOMI[**]

[**]Department of Mechanical Engineering, The University of Tokyo,
7-3-1 Hongo, Bunkyo-ku, Tokyo 113-8656, JAPAN
E-mail: maruyama@photon.t.u-tokyo.ac.jp

Abstract

Heat transfer of single-walled carbon nanotubes (SWNTs) in practical situations is investigated using molecular dynamics (MD) simulations. Attenuation of the expected high thermal conductivity was simulated by mixing ^{13}C isotope impurities to SWNTs or binding two SWNTs with different chirality with a junction structure in between. The heat transfer through the junction can be expressed with the thermal boundary conductance by considering a virtual boundary at the junction. The lateral heat conduction was compared with the thermal boundary conductance at the interfaces between an SWNT and surrounding materials. By applying the lumped capacity method on the non-stationary molecular dynamics simulations, the thermal boundary conductance of an SWNT bundle and an SWNT confining water were calculated. Finally, some conventional properties were estimated to characterize the anisotropic heat conduction.

Key words: Carbon Nanotube, Molecular Dynamics, Heat Conduction, Thermal Boundary conductance, Fin Efficiency

1. Introduction

Single-walled carbon nanotubes (SWNTs) [1] have remarkable electrical, optical, mechanical and thermal properties [2, 3]. On investigating the thermal properties of SWNTs, the classical molecular dynamics (MD) simulations serve as strong tools since the heat transfer is mainly governed by phonon transport. Utilizing MD simulations, much of the recent attention has been paid to the lateral thermal conduction which is expected to be extremely high [4]. Furthermore, the thermal conductivity shows strong dependence on the nanotube length for realistic length scale in the device applications [5, 6].

Despite the expected high thermal conductivity of pure and defect-free SWNTs, in practical situations, SWNTs may contain some impurities and defects which enhance the phonon scattering hence attenuate the heat conduction. One apparent example of impurities in SWNTs would be the carbon isotopes. Since minute mixture of carbon isotopes in diamond is known to cause large reduction in thermal conductivity [7], investigating the isotope effect on carbon nanotubes is of a strong interest. On the other hand, when SWNTs contain defects, the local irregular lattice structures should certainly be a strong potential for local thermal resistances. A case of such local defective structures is the chirality junction where two SWNTs with different chirality and radius are connected through certain transitional lattice structures. Such junctions can be found in the actual growth process [8], and the junction structure can be uniquely determined for given chiral vectors of an SNWT pair [9].

On considering practical applications of SWNTs as electrical devices and composite materials, characterization of their anisotropic heat transfer is of a prior importance, as the

acceptable heat load would be limited by the thermal resistance to the surrounding mediums. One of the essential systems to consider in this course is an SWNT bundle, as grown nanotubes usually form bundles. As the inter-tube heat transfer is governed by the weak van der Waals force, the system is expected to show strongly anisotropic heat transfer with relatively small inter-tube thermal boundary conductance. Once the inter-tube heat transfer is identified, it would be natural to extend the study to investigate the thermal conductance between SWNT and some omnipresent materials such as water. Furthermore, as there are ongoing extensive research on the water in an SWNT in connection with its anomalous phase change in the nanoscale quasi-one-dimensional confinement [10], characterization of heat conduction should hold certain interest.

The current paper aims to provide results from series of molecular dynamics simulations in order to characterize the anisotropic thermal properties of SWNTs in practical situations with effects of impurities and defects. Firstly, we investigate the attenuation of the thermal conductivity due to the isotope impurities and chirality junctions. Secondly, the heat transfer from an SWNT to various surrounding materials is simulated. Heat transfer between SWNTs in a bundle of nanotubes and between water and an SWNT are considered. In both interfacial systems, the heat transfer rate can be well expressed by the thermal conductance at the boundary. Finally, the anisotropic heat transfer of SWNTs is characterized by comparing the axial and radial heat conduction.

2. Simulation Methods

2.1 Potential Functions

The Brenner potential [11] with the simplified form [12] is employed as the potential function between carbon and carbon within a nanotube. This potential can describe variety of small hydrocarbons, graphite and diamond lattices. The basic formulation of the potential is based on the covalent-bonding treatment developed by Tersoff [13]. The total potential energy of the system E_b is expressed as the sum of the bonding energy of each bond between carbon atoms i and j.

$$E_b = \sum_i \sum_{j(i<j)} \left[V_R(r_{ij}) - B_{ij}^* V_A(r_{ij}) \right], \tag{1}$$

where $V_R(r)$ and $V_A(r)$ are repulsive and attractive force terms, respectively. The Morse type form with a cut-off function $f(r)$ expresses these terms.

$$V_R = f(r) \frac{D_e}{S-1} \exp\left\{ -\beta\sqrt{2S}(r - R_e) \right\}, \tag{2}$$

$$V_A = f(r) \frac{D_e S}{S-1} \exp\left\{ -\beta\sqrt{2/S}(r - R_e) \right\}, \tag{3}$$

$$f(r) = \begin{cases} 1 & (r < R_1) \\ \frac{1}{2}\left(1 + \cos\frac{r - R_1}{R_2 - R_1}\pi\right) & (R_1 < r < R_2) \\ 0 & (r > R_2) \end{cases} \tag{4}$$

The effect of the bonding condition of each atoms is taken into account through B_{ij}^* term which is the function of angle θ_{ijk} between bonds i-j and i-k,

$$B_{ij}^* = \frac{B_{ij} + B_{ji}}{2}, \quad B_{ij} = \left(1 + \sum_{k(\neq i, j)} G_c(\theta_{ijk}) f(r_{ik})\right)^{-\delta}, \tag{5}$$

where

Table 1.   Parameters for Brenner potential.

D_e [eV]	R_e [Å]	S	R_1 [Å]	R_2 [Å]
6.0	1.39	1.22	1.7	2.0
β [Å^{-1}]	δ	a_0	c_0	d_0
2.1	0.5	0.00020813	330	3.5

$$G_c(\theta) = a_o \left(1 + \frac{c_o^2}{d_o^2} - \frac{c_o^2}{d_o^2 + (1+\cos\theta)^2} \right). \tag{6}$$

The constants are shown in Table 1. Here, we have employed the parameter set II (table 2 in [11]), which reproduces the force constant better. Here, we have ignored [12] the term for the conjugate bond from original expressions of Brenner. The velocity Verlet method was adopted to integrate the equation of motion with the time step of 0.5 fs.

In case of simulating an SWNT bundle, in addition to the Brenner potential between carbon atoms within an SWNT, van der Waals force between carbon atoms in different SWNTs was expressed as 12-6 Lennard-Jones potential with parameters in Table 2.

On investigating the heat transfer at the boundary between an SWNT and confined water molecules, the Brenner potential was used between carbon and carbon. Water molecules were expressed by SPC/E potential [14]. SPC/E potential is expressed as the superposition of Lennard-Jones function of oxygen-oxygen interaction and the electrostatic potential by charges on oxygen and hydrogen as follows.

$$\phi_{12} = 4\varepsilon_{OO} \left[\left(\frac{\sigma_{OO}}{R_{12}} \right)^{12} - \left(\frac{\sigma_{OO}}{R_{12}} \right)^6 \right] + \sum_i \sum_j \frac{q_i q_j e^2}{4\pi\varepsilon_0 r_{ij}}, \tag{7}$$

where R_{12} represents the distance of oxygen atoms, and σ_{OO} and ε_{OO} are Lennard-Jones parameters. The Coulombic interaction is the sum of 9 pairs of point charges. The potential was simply cut off at a distance of 25 Å. The potential energy between two water molecules with a distance of 25 Å was calculated to be 0.043 kJ/mol at maximum and -0.042 kJ/mol at minimum, which is considered to be small enough not to have significant influence on the interfacial heat conduction. The potential function between water molecules and carbon atoms are represented by Lennard-Jones function (with parameters in Table 2) and the quadrupole interaction term,

$$\phi(r) = \frac{1}{3} \frac{q}{4\pi\varepsilon_0} \sum_{\alpha,\beta} \Theta_{\alpha,\beta} \frac{3r_\alpha r_\beta - r^2 \delta_{\alpha\beta}}{r^5}, \tag{8}$$

where α and β run over the Cartesian coordinates x, y, z, and r is the distance between the charge site and the quadrupole carbon site and $\delta_{\alpha,\beta}$ is the delta function [15, 16]. The quadrupole moment tensor is given by,

$$-2\Theta_{x'x'} = -2\Theta_{y'y'} = \Theta_{z'z'} = -3.03 \times 10^{-40} C^2, \tag{9}$$

where x', y' and z' denote the local coordinate system centered at the quadrupole site with z' being the wall normal direction.

2.2 Thermal Conductivity Measurements

In our previous reports [5, 6], thermal conductivity was calculated from the measured temperature gradient and the heat flux obtained by the energy budgets of phantom molecules. After obtaining the average temperature of about 300 K or 100 K with the auxiliary velocity scaling control, simulations with only the phantom temperature control were performed for typically 1 ns in order to achieve the equilibrium. Then, for the quasi-stationary state with the temperature difference of 20 K, the measurement

Table 2. Parameters for Lennard-Jones potentials.

	σ [nm]	ε [meV]
Carbon-Carbon	0.337	2.400
Carbon-Water	0.319	0.674

of the temperature distribution was carried out for typically 10 ns. From energy budgets of controlling phantom molecules, the heat flux along the tube can be simply calculated. Combined with the temperature gradient, the thermal conductivity λ can be calculated through the Fourier's equation,

$$q = -\lambda \frac{\partial T}{\partial z} . \qquad (10)$$

The cross-sectional area A of a nanotube can be defined in two different ways. One is to use the area of a hexagon dividing a bundle of SWNTs: $A = 2\sqrt{3}(d/2 + b/2)^2$, where b is van der Waals thickness 0.34 nm. The other definition uses the ring of van der Waals thickness: πbd, which can also be a proper one [5, 6]. The former definition is appropriate for calculating the amount of heat which can be conducted by nanotubes packed in a limited cross-sectional area. The latter definition is essential for measuring the enhancement of thermal conductivity with a double-walled carbon nanotube (DWNT) or peapod. Here, DWNT is made of 2 concentric SWNTs and peapod is an SWNT filled with fullerene. Furthermore, the latter definition is suited for comparison of SWNTs with different diameters [5, 6], because the thermal conductivity should be primarily proportional to the circumferential length of a nanotube.

The calculated thermal conductivity for finite length SWNTs was not as high as the previously reported value for the infinite length SWNT, 6600 W/mK at 300 K [4]. However, the thermal conductivity is still much higher than high-thermal conductivity metals. The dependence of the thermal conductivity on the nanotube length is shown in Fig. 1. In the length regime reported in [5, 6] ($L<0.4$ μm), the thermal conductivity showed a power-law increase with respect to the nanotube length. The observed power-law dependence gave rise to discussions on the analogy to the one-dimensional model calculations of thermal conductivity [17, 18], where λ diverges with increasing L. In the current report, we present the length effect in much wider range of tube lengths ($L<3.2$ μm) as marked with circles in Fig. 1. Recently, we have also performed simulation using Nose-Hoover thermostats to investigate the influence of thermal boundary resistances between the temperature controlled tube ends and the
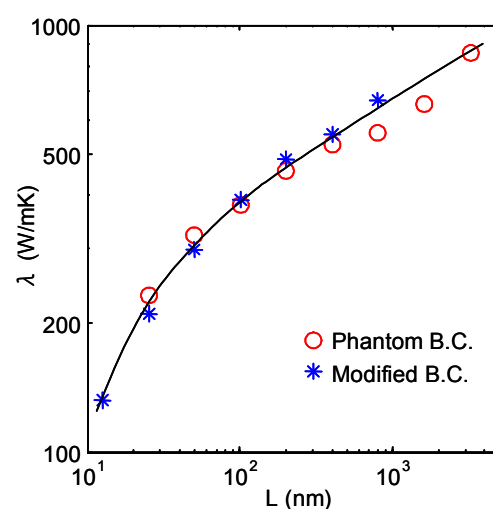

Fig. 1. Dependences of thermal conductivity on the length of nanotubes L for 300 K computed with the phantom boundary condition (B. C.) [5, 6] and modified boundary B. C. [19].

rest of the nanotube [19]. The length and relaxation time of the thermostats were tuned to minimize the thermal boundary resistances. The obtained thermal conductivity (asterisks) agrees well with that calculated using the phantom technique. The overall trend of the thermal conductivity length dependence follows the solid line in Fig. 1. Although the thermal conductivity is expected to converge when the tube length is much longer than the mean free path of phonon carrying energy, in the larger L regime in the explored parameter space (200 nm$<L<$3.2 μm), the thermal conductivity still exhibits an exponential growth.

3. Results and discussions

3.1 Isotope effects on thermal conductivity

Thermal conductivity of nanotube with randomly distributed ^{13}C with various ratios was calculated. As seen in Fig. 2, the general trend of the results shows that the thermal conductivity decreases as the number ratio of ^{13}C increases due to the enhancement of phonon scattering. Further analysis reveals that the dependence of thermal conductivity on isotope ratio can be well fit to the following equation indicated by solid lines in Fig. 2.

$$\lambda = \sqrt{\frac{12}{12(1-\beta)+13\beta}} \cdot \frac{\lambda_0}{1+C_1 \cdot \beta(1-\beta)\lambda_0} , \qquad (11)$$

where β is the number ratio of ^{13}C, λ_0 the thermal conductivity of pure ^{12}C-SWNTs and C_1 a fitting parameter. The equation can be formulated through a simple phonon collision model. Assuming effective heat capacity C_v and phonon relaxation time τ_p invariant for all the phonons with contribution to the heat conduction, the thermal conductivity can be expressed in the conventional form,

$$\lambda = \frac{1}{3} C_v \tau_p \sum_i v_i^2 . \qquad (12)$$

The simplest model of the enhancement of the phonon collision rate τ_p due to the presence of isotopes can be expressed as,

$$\frac{1}{\tau_p} = \frac{1}{\tau_{p0}} + \frac{\beta(1-\beta)}{\tau_{p1}} , \qquad (13)$$

where τ_{p0} is the collision rate of the pure ^{12}C-SWNT and τ_{p1} is a representative collision rate due to the impurities. Substituting (13) into (12) and taking the mass difference of isotopes into account, one can easily reach the expression (11) with the fitting constant C_1 being the inverse of thermal conductivity based on τ_p,

$$C_1 = \frac{3}{C_v \tau_{p1} \sum_i v_i^2} . \qquad (14)$$

The results of the current MD simulations suggest that, at room temperature, the isotope effect on the heat conduction of SWNTs is minor compared with that on the diamonds, where, for β=1 %, about 30 % thermal conductivity reduction was experimentally observed [7].
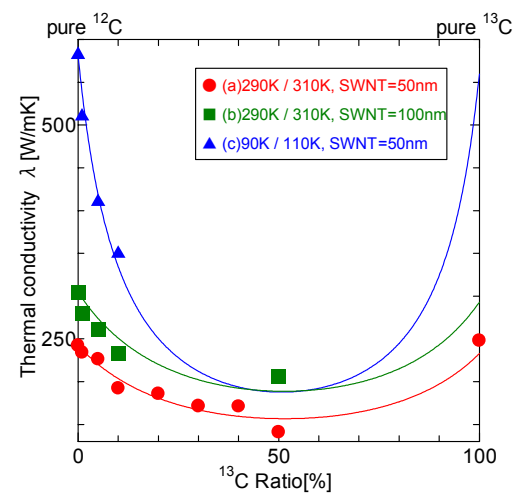

Fig. 2. Effect of ^{13}C isotope on thermal conductivity of SWNT.

Two cases with different length were simulated at 300 K in order to examine the size dependence of the isotope effect. As shown in Fig. 2, the variation of the thermal conductivity between the two results is almost constant. One could understand that the additional long wavelength phonons by lengthening the nanotube are not influenced by the isotopes whose effects are localized in relatively short atomic length scale.

The temperature dependence was tested by lowering the temperature of the 50nm nanotube to 100 K. Note that this case violates the limitation of the classical MD simulation, which cannot reproduce the correct heat capacity at low temperature [6]. Still, this type of case studies should be beneficial to gain insights in terms of molecular dynamics. The analyses allow us to probe the influence of the isotope effect on phonon mean free path. If we assume the quantum effect on the heat capacity and isotope effect on the phonon mean free path to be independent of each other at low temperature, the proper thermal conductivity can be roughly estimated by multiplying thermal conductivity calculated by the MD simulations with the ratio of reduction in heat capacity due to the quantum effect. By lowering the temperature, the phonon mean free path becomes longer due to the reduction of thermal scattering. As seen in Fig. 2, the reduction ratio does not show major dependence on the temperature, hence the current simulation results do not suggest a significant influence of the phonon mean free path on the isotope effects.

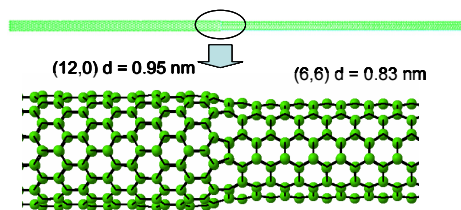
Fig. 3. Junction of two different SWNTs.

Fig. 4. Temperature jump at the junction by local increase in the thermal resistance.

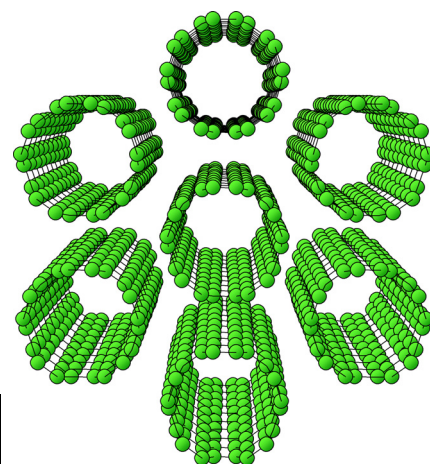### 3.2 Thermal conductance at an SWNT junction

One example of the interesting features of the system with nanotube junctions is the thermal conductance at the junction of nanotubes with different chiralities. The simulated system is shown in Fig. 3. In this case a (12, 0) zigzag nanotube on the left-hand side and a (6, 6) armchair nanotube were smoothly connected using 5-membered and 7-membered rings at the junction. By applying different temperatures at each end, temperature distribution was measured as in Fig. 4. The temperature jump at the junction

Table 3. Parameters used for calculation of the thermal conductance at SWNT junctions.

d [nm]	A [nm^2]	ΔT [K]	Q [W]
0.83194	0.889	4.05	5.16×10^{-8}

Fig. 5. Initial condition of SWNT bundle simulation.

Table 4. The characteristic length of the thermal conductance.

	S [nm^2]	$\rho_{cold}V_{cold}$ [kg]	c_{cold} [J/kgK]	$\rho_{hot}V_{hot}$ [kg]	c_{hot} [J/kgK]	K [MW/ m^{2}K]	L_{TC} [μm]
SWNT-SWNT	18	2.39×10^{-23}	1039	3.99×10^{-24}	1039	4.04	0.207
SWNT -Water	28.8	5.74×10^{-24}	1153	3.19×10^{-23}	1039	5.01	0.186

is clearly observed. This temperature jump can be modeled by assuming that there is a virtual boundary between two nanotubes with different structures. Now, we consider the thermal boundary conductance (TBC) of the virtual interface which relates the temperature drop and the heat flux through the boundary as,

$$K = \frac{Q}{A\Delta T} \ . \tag{15}$$

TBC at the junction is calculated as 1.4×10^4 MW/m^{2}K using the values in Table 3. Here, the cross-sectional area was defined as πbd. We have also tried various combinations of SWNTs whose diameter ratio ranges up to about 2. Furthermore, if we allow two connected nanotubes to be uncoaxial, various possible structures for a given pairs of SWNTs can be constructed. Although the results are not shown here, the TBC of the tested geometries falls well within an order of magnitude difference. The detailed data of this parameter study will be reported elsewhere.

3.3 Inter-tube thermal conductance in an SWNT bundle

As the initial condition, 7 SWNTs with the length of 2.51 nm were placed in a 2.51×6.0×6.0 nm simulation cell as in Fig. 5. Each SWNT was a (5, 5) armchair tube with 0.693 nm in diameter. At the beginning of the computation, the whole system was kept at 300 K for 100 ps. The inter-tube distance at equilibrium approximately corresponds to σ. Then, the temperature of only the central SWNT was suddenly increased to 400 K using the velocity scaling method for 10 ps. After that, all the temperature controls were turned off.
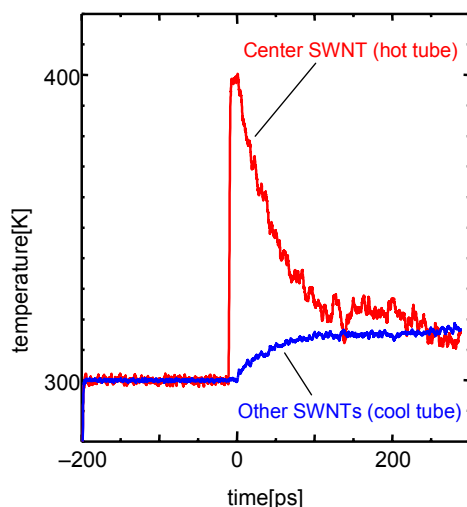

Fig. 6. Time histories of the temperature of hot (central) SWNT and cold (surrounding) SWNTs.
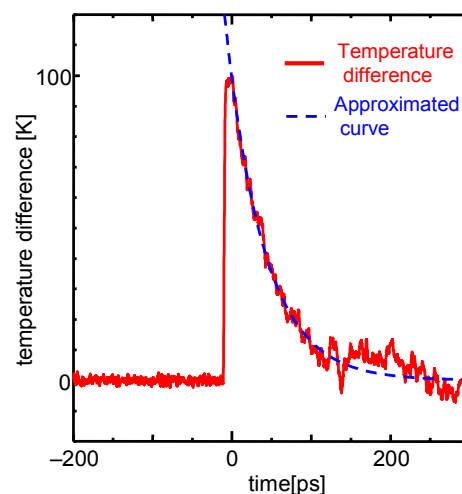
Fig. 7. Time history of the temperature difference of central and surrounding SWNTs.

Figure 6 shows a time history of the temperature difference between the hot (central) tube and cold (surrounding) tubes. Here, the heat transfer from the central tube to surrounding tubes is clearly observed. In order to examine this heat transfer, temperature difference of central and surrounding tubes is drawn in Fig. 7. The monotonic decay of the temperature difference in Fig. 7 was well approximated by an exponential function;

$$T_{hot} - T_{cold} = T_0 \exp\left(-\frac{t}{\tau}\right), \tag{16}$$

where

$$T_0 = 99.58 \text{ K}, \quad \tau = 48.7 \text{ ps}.$$

The non-stationary heat transfer problem can be simplified if the intra-tube resistance to heat transfer is small compared to the inter-tube TBC. This is the case in the current problem as the Biot number in Eq. (17) is very small with the extremely small characteristic length of an SWNT.

$$Bi = \frac{Kd}{\lambda}. \tag{17}$$

Then the lumped capacity method in Eq. (16) can be adopted,

$$T_{hot} - T_{cold} = T_0 \exp\left[-\left(\frac{1}{\rho_{hot} c_{hot} V_{hot}} + \frac{1}{\rho_{cold} c_{cold} V_{cold}}\right) KSt\right], \tag{18}$$

where ρ, c, V and S are density, heat capacity, volume and contact area, respectively. Here, S is estimate as the surface area of hexagonal cells dividing a bundle of SWNTs. Note that we have reduced a bundle of 7 SWNTs to a two body problem by assuming the homogeneous non-stationary heat transfer to the 6 surrounding SWNTs from the central one. The excellent agreement to an exponential fit by Eq. (16) in Fig. 7 shows the validity of the current analysis. Comparing Eq. (16) with Eq. (18), the thermal boundary conductance K was estimated. By using values in Table 4, TBC between SWNTs in a bundle was calculated to be about 4.04 MW/m²K.

3.4 Thermal conductance between SWNT and confined water

A (10, 10) SWNT with length of 20.1 nm containing 192 water molecules inside was prepared in the 20.1×10.0×10.0 nm fully-periodic simulation cell as in Fig. 8. In the initial stage of simulation, water molecules and the SWNT were equilibrated at temperature of 300 K. Then, only the temperature of the SWNT was suddenly heated up to 400 K. After applying the heat for 1 ps, all the temperature controls were turned off.

Figure 9 shows the temperature time evolutions of the SWNT and water molecules, where the heat transfer from heated SWNT to water is observed. On extracting the time history of the temperature difference shown in Fig. 10, just as in the case of the SWNT bundle, a clear fit to the exponential function Eq. (16) was observed with following
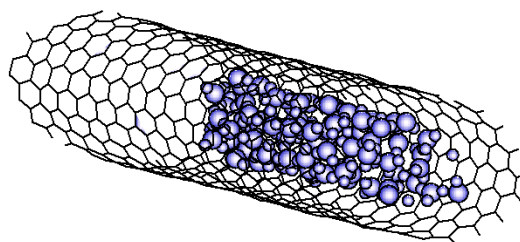

Fig. 8. An SWNT and the confined water molecules.

parameters.

$$T_0 = 85.5 \text{ K}, \quad \tau = 38.2 \text{ ps} .$$

K is estimated to be 5.01 MW/m^{2}K using the lumped capacity method similarly to the case of the SWNT bundle simulations.

3.5 Anisotropic heat transfer of SWNTs

The above results indicate that even with isotope impurities and junctions, the carbon nanotube heat transfer is strongly anisotropic. Note that TBC computed for the chirality junction is several orders larger than that for the SWNT bundle and water confined SWNT. Here, by taking the representative value of the axial thermal conductivity of SWNT as 1000 W/mK, we characterize the anisotropic heat transfer of SWNTs. Now, by balancing the axial and radial heat conduction as,

$$\frac{A\lambda}{L} = KS , \tag{19}$$

we can estimate the characteristic length of the thermal conductance at the boundary based on the axial thermal conductivity. By denoting this characteristic length of TBC as (L_{TBC}), we obtain,

$$\frac{\left(\frac{\pi}{4} d^2\right)\lambda}{L_{TBC}} = \left(\pi d L_{TBC}\right)K , \tag{20}$$

hence,

$$L_{TBC} \equiv \frac{1}{2}\sqrt{\frac{\lambda d}{K}} . \tag{21}$$

By using Eq. (21), L_{TBC} is calculated to be 0.207 μm as shown in Table 4. In other words, when the length of SWNT is 0.207 μm, the thermal conductance in axial direction and that in radial direction balance. Suppose one uses an SWNT as a promoter of heat conduction as a composite material, inter-tube TBC determines the performance for a shorter nanotube than L_{TBC}. L_{TBC} between the SWNT and water molecules is also calculated using Eq. (21) as 0.186 μm.
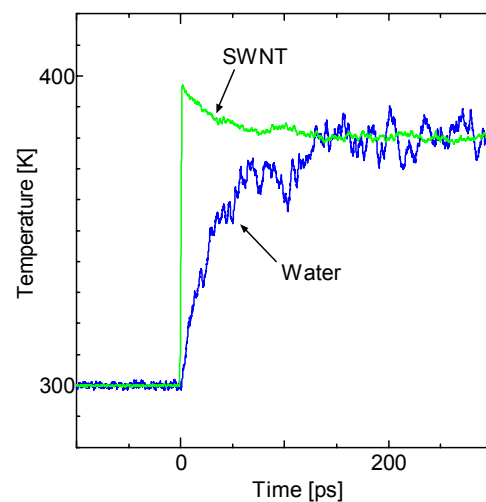

Fig. 9. Time histories of the SWNT and water temperature.
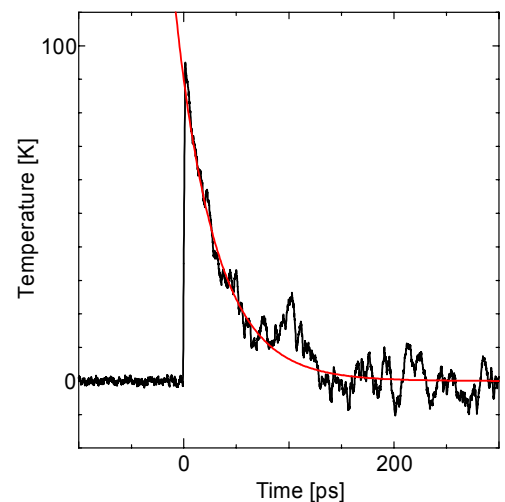

Fig. 10. Time history of the temperature difference of SWNT and confined water.

In course of promotion of heat conduction in engineering applications, one may think of attaching one end of SWNT bundles to the heat source to use them as fins. One of the key issues here to optimize the cost of material would be the dependence of the efficiency of the fins on the tube length. This can be characterized by the fin efficiency,

$$\eta_f = \frac{\tanh L\beta}{L\beta},$$

$\qquad(22)$

where the parameter β in this case is expressed as,

$$\beta = \sqrt{\frac{\pi dK}{\lambda A}} = \sqrt{\frac{4K}{\lambda d}}.$$

$\qquad(23)$

Since thermal conductivity of finite SWNTs exhibit distinct size effect, the length dependence of the efficiency can not be purely characterized by a universal value of β. For the representative value of thermal conductivity, 1000 W/mK, β can be calculated to be 4.83 μm^{-1}.

4. Conclusions

Anisotropic heat transfer of SWNTs was characterized based on molecular dynamics simulations. The expected high thermal conductivity can be reduced by randomly mixing ^{13}C isotopes, where the reduction increases with the number ratio of the mixed isotopes following the trend matches with a simple phonon collision model. The axial heat conduction can also be hindered by the chirality junctions, where the local irregular lattice structure gives rise to a jump in the temperature profile at the boundary. These effects, however, are still minute compared with the radial heat transfer through the wall interfaces to other SWNTs or confined water. By using the lumped capacity method, thermal boundary conductance (TBC) at SWNT-SWNT and water-SWNT interfaces was estimated. Finally, the anisotropic heat conduction was characterized by adopting some of the engineering properties. The characteristic length scale of TBC is calculated to be 0.207 μm in the SWNT bundle case, and 0.186 μm in the SWNT and water molecules case, respectively.

Acknowledgments

References

(1) Iijima, S. and Ichihashi, T., Single-Shell Carbon Nanotubes of 1-nm Diameter, *Nature*, Vol.363 (1993), pp. 603-605.
(2) Dresselhaus, M.S. et al., Science of Fullerenes and Carbon Nanotubes, (1996), Academic Press, New York.
(3) Saito, R., et al., Physical Properties of Carbon Nanotubes, (1998), Imperial College Press, London.
(4) Berber, S. et al., Unusually High Thermal Conductivity of Carbon Nanotubes, *Physical Review Letters*, Vol.84 (2000), pp. 4613-4616.
(5) Maruyama, S., A Molecular Dynamics Simulation of Heat Conduction in Finite Length SWNTs, *Physica B*, Vol. 323 (2002), pp. 193-195.

(6) Maruyama, S., A Molecular Dynamics Simulation of Heat Conduction of a Finite Length Single-Walled Carbon Nanotube, *Journal of Microscale Thermophysics Engineering*, Vol. 7 (2003), pp. 41-50.

(7) Onn, D.G. et al., Some aspects of the thermal conductivity of isotopically enriched diamond single crystals, *Physical Review Letters*, Vol. 68 (1992), pp.2806-2809.

(8) Iijima, S. et al., Pentagons, heptagons and negative curvature in graphite microtubule growth, *Nature*, Vol. 356 (1992), pp. 776.

(9) Saito, R. et al., Tunneling conductance of connected carbon nanotubes, *Physical Review B*, Vol. 53 (1996), pp. 2044-2050.

(10) Koga, K. et al., Formation of ordered ice nanotubes inside carbon nanotubes, *Nature*, Vol 412 (2001), pp. 802-805.

(11) Brenner, D.W., Empirical Potential for Hydrocarbons for Use in Simulating the Chemical Vapor Deposition of Diamond Films, *Physical Review B*, Vol. 42 (1990), pp. 9458-9471.

(12) Yamaguchi, Y., Maruyama, S., A Molecular Dynamics Simulation of the Fullerene Formation Process, *Chemical Physics Letters*, Vol. 286 (1998), pp. 336-342.

(13) Tersoff, J., New empirical model for the structural properties of silicon, *Physical Review Letters*, Vol. 56, (1986), pp. 632-635.

(14) Berendsen, H.J.C. et al., The missing term in effective pair potentials, *Journal of Physical Chemistry*, Vol. 91-24 (1987), pp. 6269-6271.

(15) Hansen, F. Y., Molecular-dynamics study of the dynamical excitations in commensurate monolayer films of nitrogen molecules on graphite: A test of the corrugation in the nitroger-graphite potential, *Physical Review B*, Vol. 51 (1995), pp. 2515-2536.

(16) Walther, J.H. et al., Carbon Nanotubes in Water: Structural Characteristics and Energetics, *Journal of Physical Chemistry B*, Vol. 105 (2001), pp. 9980-9987.

(17) Livi, R., Lepri, S., Heat in One Dimension, *Nature*, Vol. 421 (2003), pp. 327-327.

(18) Lepri, S., Memory Effects and Heat Transport in One-Dimensional Insulators, *European Physics Journal B*, Vol. 18, (2000), pp. 441-446.

(19) Maruyama, S., Shiomi, J., Molecular Dynamics of Phonon Transport in Finite-Length Single-Walled Carbon Nanotubes (To be submitted).